Communication in Physical Sciences, 2026, 13(2): 223-245

Comparative study on batch adsorption of Pb^{2+}, Cd^{2+} and Ni^{2+} onto corn cob charcoal and activated silica: Kinetic and Characterization studies

John Chukwubuikem Ariwa, Okoche Kelvin Amadi*, Innocent Ajah Okoro and Nnedimma Immaculate Onaka

Received: 12 December 2025/Accepted: 9 February 2026 /Published: 20 February 2026
https://dx.doi.org/10.4314/cps.v13i2.5

Abstract: *Heavy metal contamination of water poses serious environmental and health risks/ Therefore, this study aims to evaluate the efficiency of charcoal and activated silica as low-cost adsorbents for the removal of Pb(II), Cd(II), and Ni(II) ions from aqueous solutions. The effects of pH, temperature, and contact time on adsorption were systematically evaluated. For silica, the maximum adsorption capacities were 7.50 mg/g for Pb(II), 7.50 mg/g for Cd(II), and 7.50 mg/g for Ni(II), while for charcoal, the corresponding capacities were 7.50 mg/g, 7.50 mg/g, and 7.51 mg/g, respectively. Optimal adsorption occurred at pH 4 for Pb(II) and pH 6 for Cd(II) and Ni(II), with maximum removal efficiencies of 86.44%, 80.34%, and 71.56% for silica and 96.34%, 90.49%, and 92.75% for charcoal. Adsorption kinetics were evaluated using pseudo-first-order, pseudo-second-order, and intraparticle diffusion models, with the pseudo-second-order model providing the best fit ($R^2 = 1.000$), indicating chemisorption-dominated processes. Intraparticle diffusion analysis suggested that adsorption was particle-diffusion controlled, with boundary layer thickness (X_i) ranging from 7.46 to 7.47 mg/g. The results demonstrate that both adsorbents, particularly charcoal, are highly effective for the removal of Pb(II), Cd(II), and Ni(II) ions and hold potential for the treatment of industrial wastewater.***

Keywords: *Adsorption, silica, charcoal, Heavy Metals, Pollution.*

John Chukwubuikem Ariwa
Department of Chemistry, Michael Okpara University of Agriculture, Umudike, P.M.B. 7267, Umuahia, Abia State, Nigeria
Email: zubyyte@gmail.com

Okoche Kelvin Amadi
Department of Chemistry, Michael Okpara University of Agriculture, Umudike, , P.M.B. 7267, Umuahia, Abia State, Nigeria
Email: amadikelvin77@gmail.com
https://orcid.org/0000-0001-5101-6799

Innocent Ajah Okoro
Department of Chemistry, Michael Okpara University of Agriculture, Umudike, P.M.B. 7267, Umuahia, Abia State, Nigeria
Email: okoroia@yahoo.com

Nnedimma Immaculate Onaka
Department of Chemistry, Michael Okpara University of Agriculture, Umudike, P.M.B. 7267, Umuahia, Abia State, Nigeria
Email: onakannedimma@gmail.com

1.0 Introduction:

Water is a vital natural resource essential for human survival, socio-economic development, and ecosystem sustainability. Access to safe and clean drinking water is fundamental to public health and environmental protection. Water is a ubiquitous solvent and a primary cause of infectious illnesses (Ai *et al*., 2011. The primary sources of water contamination include runoff from residential and commercial wastewater, air deposition, storage tank leaks, ocean dumping, industrial wastes, corrosion products, pharmaceutical wastes and radioactive waste (Batheja *et al*., 2009; Bademo *et al*., 2016; Eddy *et al*., 2023a-d;

Eddy *et al*., 2008). Industrial wastes and heavy metals that have been discarded end up in lakes and rivers, where they can harm both people and wildlife. Industrial wastes contain toxins that can lead to acute poisoning, immunosuppression, and reproductive failure. Contaminated water can spread infectious diseases such as cholera, typhoid fever, gastroenteritis, diarrhea, vomiting, skin infections, and kidney disease (Pal *et al*., 2018). While certain metals naturally oppose the vital functions of other elements, human activity has resulted in a substantial pollution load that surpasses the aquatic environment's ability to clean itself (Zacaroni *et al*., 2015. In small amounts, the body requires a variety of trace elements and heavy metals like zinc, copper, iron, manganese, and cobalt (Lane *et al*., 2000); while they are toxic at higher concentrations (Chronopoulos *et al*., 1997). However, several non-essential heavy metals, including lead (Pb), cadmium (Cd), chromium (Cr), mercury (Hg), and nickel (Ni), are highly toxic even at low concentrations and pose significant risks to human health The poisonous heavy metal ions first enter the human body through the food chain (Merzouk *et al*., 2011). Because heavy metals are not biodegradable, they stay in the human body permanently for a considerable amount of time (Awaka-Ama *et* al., 2024; Hahladakis *et al*., 2013; Diagomanolin *et al*., 2004). Three prevalent hazardous heavy metals to which human is exposed more and more are lead, nickel and cadmium, because of their wide range of applications in materials and technologies that are essential to human survival. The World Health Organization (WHO) recommends a maximum permissible limit of 10 μg L^{-1} for Pb^{2+} in drinking water, due to its cumulative toxicity and adverse neurological effects. (World Health Organization, 2000). Cadmium is one of the more poisonous metals, with intake causing several symptoms such as high blood pressure, renal damage, and red blood cell destruction (Ghazy, 1995; Ghazy *et al*., 2008b). The methods for treating wastewater include separation, coagulation/flocculation, precipitation, ion exchange, electrocoagulation, reverse osmosis, and adsorption (ref). Among these methods, adsorption remains one of the most effective and widely applied techniques for heavy metal removal due to its high efficiency, operational simplicity, and economic feasibility.. Adsorption has been confirmed to be excellent for different methods of water purification in terms of ease of application, cost, simplicity of design, and viability for in situ treatment of underground and surface water. Adsorption is a surface phenomenon where molecules, atoms, or ions from a gas, liquid, or dissolved solid cling to the adsorbent's active site to form an adsorbate film on the adsorbent's surface. The process of removing a substance from a liquid or gas by means of a solid phase that results in a larger concentration (or accumulation) of removed adsorbate molecules on the adsorbent surface compared to that in the bulk of the solution is known as adsorption (Soliman & Moustafa, 2020). Furthermore, because adsorption does not require expert maintenance or equipment, it can be used in rural regions (Mizuta *et al*., 2004; Batheja *et al*., 2009). An effective adsorbent is expected to possess high abrasion resistance, good thermal stability, large surface area, and a well-developed pore structure, all of which enhance adsorption efficiency. Additionally, the adsorbents need to have a unique pore structure that allows the gaseous vapors to be transported quickly (Dureja *et al*., 2007).

A number of materials have been synthesized and used for the adsorption of Cd(II), Ni(II) and Pb(II) ions such as amino propyl-modified mesoporous carbon (Guesmi et a., 2015); low cost adsorbent (Yeganeh *et al*., 2019), chemically modified polyacrylonitrile-based fiber (Deng *et al*., 2016), nanoparticles (Eddy *et al*., 2024a-d) and spherical mesoporous silica (Zhu *et al*., 2015; Li *et al*., 2015). Although

these materials have demonstrated varying degrees of adsorption efficiency, many of them are associated with high production costs, complex synthesis procedures, or limited availability, which restrict their large-scale application, particularly in developing countries. Despite extensive studies on the adsorption of Pb(II), Cd(II), and Ni(II) ions using different synthetic and natural adsorbents, there remains limited comparative information on the adsorption kinetics, transport mechanisms, and performance of agricultural waste-derived charcoal relative to conventional adsorbents such as activated silica under identical experimental conditions. In addition, systematic characterization-based correlations between adsorbent properties and metal ion uptake are scarcely reported.

The increasing environmental and health challenges posed by toxic heavy metal pollution as the advancement in industrialization reaches the shores of the developing economies requires that more investigations should be carried out with respect to the use of commercial activated carbon adsorbents for those heavy metal ions that are prevalent in these countries (Bilal *et al*., 2021). Hence, this study aims to comparatively evaluate the batch adsorption behavior of Pb(II), Cd(II), and Ni(II) ions onto corn cob-derived charcoal and activated silica from aqueous solutions.

Activated charcoal and silica gel were used as adsorbent for this study. Characterizations of both physical and chemical properties of them will be investigated to give insight on the material and this will be used to correlate with the ions uptake in aqueous phase. In addition, Cd(II), Ni(II) and Pb(II) ions kinetic and equilibrium sorption as well as the modelling of the transport of the three ions onto the surface of the activated charcoal and silica gel will be investigated.

The findings of this study are expected to provide valuable insight into the potential application of low-cost and locally available adsorbents for heavy metal remediation, thereby contributing to sustainable wastewater treatment strategies and environmental protection in developing economies.

2. 0 Materials and Methods

2.1. Reagents and chemicals

Deionized water was used throughout the study for the preparation of all solutions and for all experimental procedures. Standard stock solutions (1000 ppm) of Pb^{2+}, Cd^{2+}, and Ni^{2+} were prepared from cadmium nitrate [$Cd(NO_3)_2$], lead nitrate [$Pb(NO_3)_2$], and nickel sulfate [$NiSO_4$], respectively, each dissolved in 0.5 mol L^{-1} HNO_3. Acidification of the stock solutions was carried out to prevent metal ion hydrolysis. Working solutions of the desired concentrations were obtained by appropriate dilution of the stock solutions with deionized water. In addition, a wastewater sample was employed to evaluate the efficiency of the developed adsorbents for heavy metal removal under practical conditions.

2.2. Preparation of the Charcoal

Corn cob (CC) was collected from Orie Ugba market (Umuahia), washed with distilled water, and oven-dried at 70 °C until a constant weight was achieved (approximately 48 h). The dried corn comb was crushed using a pulverizer and the resulting powder was packed in sealed bags and stored in a desiccator at room temperature until further use. All chemicals in this study were of analytical grades. The corn cob powder was pyrolyzed in a tubular furnace at 500 °C for 2 h under a limited oxygen flow rate of 60 mL min. The resulting charcoal was cooled to room temperature, washed with distilled water, filtered, and dried at 70°C until a constant weight was achieved (Abdel-Salam *et al*., 2025; Abuzaid *et al*., 2025). The charcoal was then ground and stored in airtight polyethylene bags before further applications.

2.3. Chemical Activation of Adsorbent (Silica)

Pure chromatographic grade silica (mesh size 60-200 μm) was soaked in excess 0.3 M HNO_3.

Acid treatment was employed to enhance surface acidity, remove surface impurities, and increase adsorption efficiency. The mixture was stirred for 30 min and kept for 24h to remove any debris or soluble bio-molecule that might interact with the metal ions during the sorption process. This treatment constituted the chemical activation of the silica adsorbent and facilitated pore opening, thereby improving its surface properties. The adsorbent was then filtered through Whatman No.11 filter paper and rinsed with de-ionized water. The rinsed adsorbent was later air dried for 12 h and stored in air tight container. The activated silica was stored in a desiccator prior to use to prevent moisture uptake.

2.4. Characterization of activated charcoal and silica adsorbents

The adsorbents were characterized using scanning electron microscopy coupled with energy dispersive X-ray analysis (SEM–EDX, JSM-IT200) and Fourier transform infrared spectroscopy (FTIR, Shimadzu Tracer-100).

2.5. Batch Adsorption experiment

All the reagents used were of analytical reagent grade and were used without further purification. The silica adsorbent was chemically activated as described in Section 2.3, while the charcoal was prepared via controlled pyrolysis without further chemical activation. Distilled deionized water was used in the preparation of all sample solutions. 30 mg/L solution of lead, cadmium and nickel used for the analysis were prepared from their salts, $Pb(NO_3)_2$, $CdSO_4$ and $NiSO_4.6H_2O$ respectively. The effect of solution pH on metal ion adsorption was investigated by adding 25 cm^3 of 30 mg L^{-1} Pb^{2+}, Cd^{2+}, or Ni^{2+} solutions into separate 100 mL conical flasks containing 0.1 g of each adsorbent and then adjusting the pH of the solutions from pH 2 to 10 using either 0.1 M HCl or 0.1 M NaOH solution and at a fixed temperature of 30^0C. The flasks were agitated for 1 h and then filtered rapidly. The residual metal ion concentration in the filtrate was finally determined using UNICAM (solar AAS 969) atomic absorption spectrophotometer. The influence of temperature on the adsorption experiment was performed in a constant speed shaking water bath by measuring 25 cm^3 of 30 mg/L portion of each of the Pb^{2+}, Cd^{2+} and Ni^{2+} solutions into several 100 cm^3 Erlenmeyer flasks containing 0.1 g of each of silica and charcoal adsorbent. The flasks were corked and agitated intermittently in a rotary shaker at different temperatures of 30ºC, 40ºC, 50 ^{0}C, 60ºC and 70ºC for 60 min and at a pH of 4 for lead and 6 for cadmium and nickel. At the end of the equilibration time, the content of each flask was filtered and the filtrate collected into different sample bottles and the residual concentration was analysed using UNICAM atomic absorption spectrophotometer (Solar AAS 969). The concentration of metal ions adsorbed was calculated as the difference between the initial and the residual concentration at the end of the adsorption process. The effect of contact time was investigated by measuring 25 cm^3 of 30 mg/L portion of each of the Pb^{2+}, Cd^{2+} and Ni^{2+}solutions into several 100 cm^3 Erlenmeyer flasks containing 0.1 g of each of silica and charcoal adsorbent. The flasks were corked and agitated intermittently in a rotary shaker at different contact times ranging from 10 min to 150 min and at a temperature of 30ºC and pH of 4 for lead and 6 for cadmium and nickel. At the end of each sorption contact time, the content of each flask was filtered and the filtrate collected into different sample bottles and the residual concentration analyzed using UNICAM atomic absorption spectrophotometer (Solar AAS 969). The concentration of metal ions adsorbed was calculated as the difference between the initial and the residual concentration at the end of each contact time.

The amount of metal ion adsorbed per unit mass of adsorbent (q_e, mg g^{-1}) was calculated

usin equation 1 (Akpanudon & Chibuzo, 2020; Odiongenyi, 2019; Odiongenyi & Afanide, 2019)

$$q_e = \frac{(C_0 - C_e)V}{m}$$

where C_0 and C_e are the initial and equilibrium concentrations (mgL^{-1}), V is the solution volume (L), and m is the mass of adsorbent (g).

3.0. Results and Discussion

3.1. Characterization of activated charcoal and silica

3.1.1. FTIR analysis

Fourier Transform Infrared (FTIR) spectroscopy was employed to identify the surface functional groups of the adsorbents and to compare their structural changes before and after Pb(II) adsorption. The FTIR spectra of activated silica gel, Pb(II)-loaded silica, activated charcoal, and Pb(II)-loaded charcoal are presented in Figs 1 to 4, respectively.

The FTIR spectrum of activated silica (Fig.1) exhibits characteristic absorption bands at 3462 cm^{-1}, 1647 cm^{-1}, 1055 cm^{-1} (very strong), 977 cm^{-1} (medium), and 794 cm^{-1}. The broad band at 3462 cm^{-1} is attributed to the stretching vibration of surface silanol (Si–OH) groups, while the band at 1647 cm^{-1} corresponds to the bending vibration of adsorbed water (H–O–H). The intense band at 1055 cm^{-1}, together with the shoulder at 977 cm^{-1}, is characteristic of the asymmetric stretching vibration of the Si–O–Si siloxane framework, whereas the band at 794 cm^{-1} is assigned to the symmetric stretching vibration of Si–O–Si linkages (Donia *et al*., 2009; Han *et al*., 2005). These features confirm the dominance of silanol and siloxane groups on the activated silica surface, which are known to serve as active sites for metal ion adsorption.

Following Pb(II) adsorption, the FTIR spectrum of Pb(II)-loaded silica (Fig. 2) shows noticeable changes when compared with that of the pristine silica. These include slight shifts, intensity reduction, and partial disappearance of the Si–O–Si asymmetric stretching band around 1055 cm^{-1}, as well as modifications in the hydroxyl-related bands at 3462 cm^{-1} and 1647 cm^{-1}. The observed spectral variations indicate the involvement of silanol and siloxane groups in Pb(II) binding. A comparative evaluation of Figs. 1 and 2 suggest that metal–silicate interactions predominantly occur through the Si–O–Si asymmetric stretching region, confirming the formation of surface metal–oxygen complexes on the silica matrix.

The FTIR spectrum of activated charcoal (Fi3) differs markedly from that of silica, reflecting its carbonaceous nature. Prominent bands are observed at 1561 cm^{-1}, 1364 cm^{-1} (very strong), 1010 cm^{-1} (medium), 764 cm^{-1}, and 689 cm^{-1}. The band at 1561 cm^{-1} is assigned to aromatic C=C stretching vibrations, while the strong band at 1364 cm^{-1} corresponds to phenolic O–H bending or C–O stretching vibrations. The band at 1010 cm^{-1} is attributed to Si–O–Si vibrations arising from mineral or ash content in the biomass-derived charcoal. The bands at 764 cm^{-1} and 689 cm^{-1} are associated with aromatic C–H out-of-plane bending vibrations, indicating the presence of substituted aromatic structures on the charcoal surface.

After Pb(II) adsorption, the FTIR spectrum of Pb(II)-loaded charcoal (Fig. 4) shows distinct spectral changes relative to the pristine charcoal. These include shifts and intensity variations in the phenolic and aromatic regions, particularly around 1364 cm^{-1} and 764 cm^{-1}. The comparative analysis of Figs. 3 and 4 indicates that Pb(II) binding on the charcoal surface is strongly associated with aromatic C–H out-of-plane bending vibrations and oxygen-containing functional groups. The observed changes at 764 cm^{-1} suggest that metal–charcoal interactions occur mainly through aromatic and phenolic surface functionalities.

A comparison of the FTIR spectra before and after Pb(II) adsorption demonstrates that while activated silica interacts with Pb(II) primarily through silanol and siloxane groups, activated charcoal binds Pb(II) predominantly via

aromatic and oxygen-containing functional groups. These differences in surface chemistry explain the observed variation in adsorption behavior between the two adsorbents**.**

3.1.2. SEM/EDX examinations

The surface morphology and elemental composition of the activated silica and corn cob charcoal adsorbents were investigated using scanning electron microscopy (SEM) coupled with energy-dispersive X-ray spectroscopy (EDX). The SEM micrographs and corresponding EDX spectra are presented in Figs. 5(a–b) for activated silica and Figs. 3.6(a–b) for activated charcoal.

The SEM image of the activated silica (Fig. 5a) reveals an irregularly aggregated structure composed of fine particles with rough and porous surfaces. The particles appear clustered, forming agglomerates of varying sizes with noticeable inter-particle voids. Such surface roughness and porosity are advantageous for adsorption processes, as they enhance surface area and provide abundant active sites for metal ion attachment. The observed morphology is characteristic of acid-activated silica materials and is consistent with enhanced adsorption performance reported in previous studies (Chakraborty *et al*., 2022).

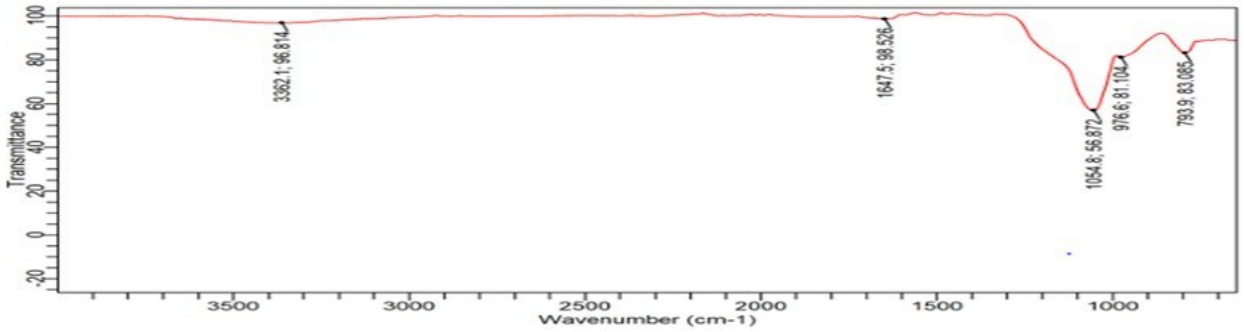

Fig. 1: FTIR spectrum of activated silica.

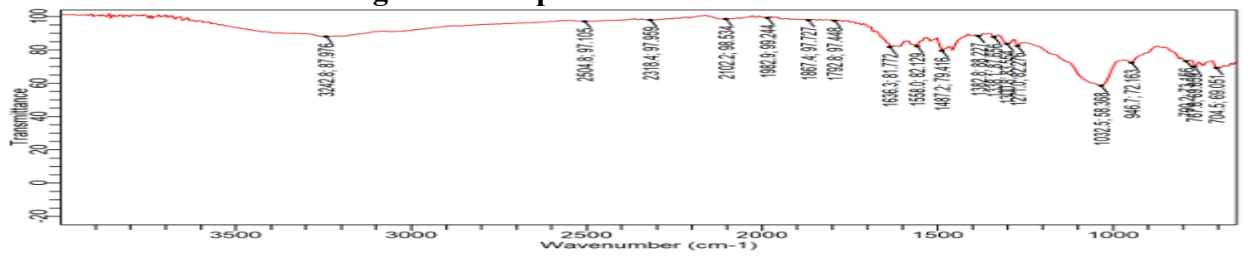

Fig/ 2: FTIR spectrum of Pb(II) loaded activated silica

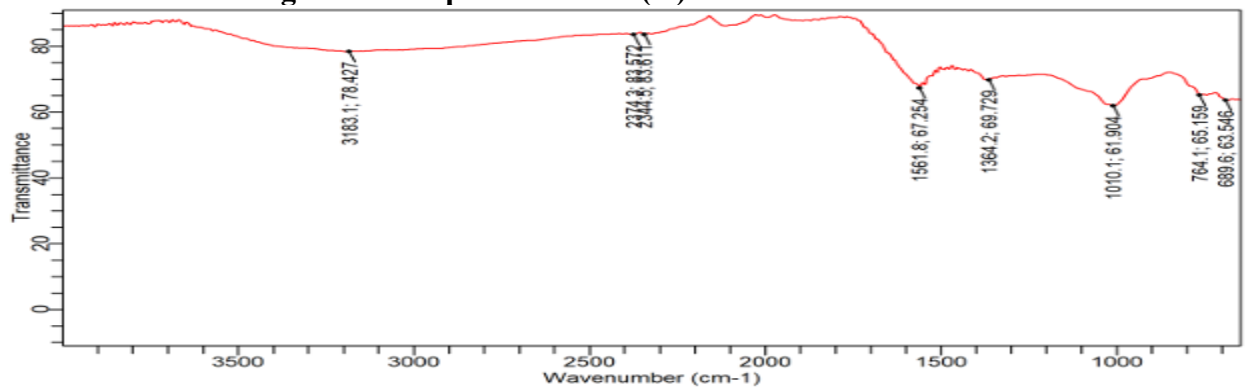

Fig. 3: FTIR spectrum of charcoal

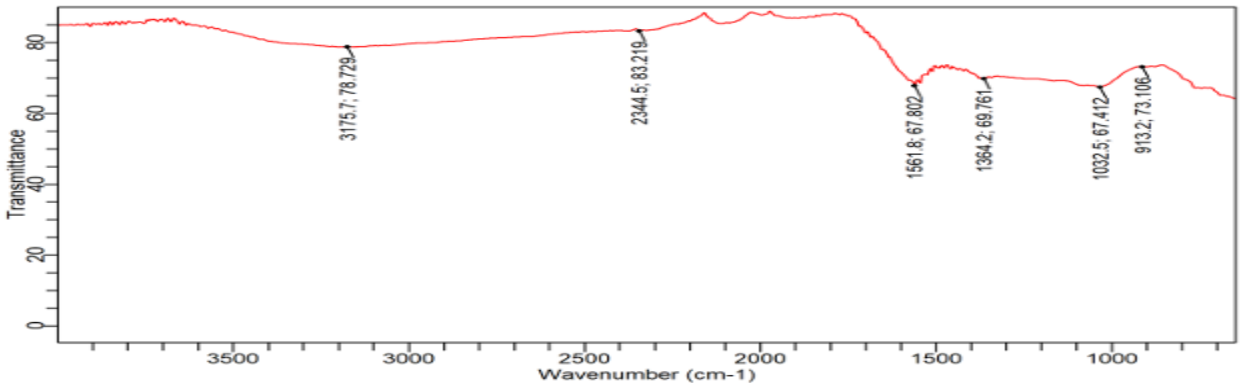

Fig. 4: FTIR spectrum for charcoal loaded with Pb(II) ions.

In contrast, the SEM micrograph of the corn cob-derived charcoal (Fig. 6a) shows comparatively well-defined, discrete, and quasi-spherical to plate-like particles with smoother edges. The charcoal particles appear more uniformly distributed, with visible pores and cavities formed during the pyrolysis process. These pores are indicative of devolatilization and carbon matrix rearrangement, which contribute to improved mass transfer and accessibility of adsorption sites. Compared to silica, the charcoal exhibits a more heterogeneous pore structure, which may facilitate multilayer adsorption and diffusion-controlled uptake of metal ions.

A comparative evaluation of the SEM images indicates that while both adsorbents possess porous morphologies conducive to adsorption, activated silica is dominated by agglomerated fine particles with surface silanol-rich regions, whereas the charcoal exhibits a more open and heterogeneous pore network arising from biomass carbonization.

The EDX spectrum of activated silica (Fig. 5b) confirms that silicon (Si) and oxygen (O) are the dominant elements, with Si accounting for approximately 71.8 wt% and O contributing about 5.4 wt%, consistent with a silica-rich matrix. Minor elemental constituents include aluminium (Al, 10.6 wt%), magnesium (Mg, 3.2 wt%), calcium (Ca, 4.3 wt%), potassium (K, 4.2 wt%), sodium (Na, 1.3 wt%), and iron (Fe, 2.5 wt%). These minor elements are likely derived from precursor impurities or residual mineral phases and may contribute synergistically to adsorption through additional surface heterogeneity.

For the activated charcoal (Fig. 6b), the EDX analysis reveals a markedly different elemental distribution. Carbon (C) is the predominant element, constituting approximately 25.8 wt%, followed by oxygen (O, 21.4 wt%) and silicon (Si, 40.6 wt%). The relatively high silicon content suggests the presence of silica-rich ash inherited from the corn cob biomass. Aluminium (Al, 8.6 wt%) and trace elements such as sodium (Na, 2.2 wt%), magnesium (Mg, 0.9 wt%), manganese (Mn, 0.9 wt%), calcium (Ca, 1.0 wt%), iron (Fe, 2.0 wt%), and silver (Ag, 0.3 wt%) were also detected.

A comparative assessment of the EDX results highlights clear compositional differences between the two adsorbents. Activated silica is dominated by silicon-based phases with abundant oxygen, supporting the FTIR-observed prevalence of silanol and siloxane functional groups responsible for surface complexation with Pb(II) ions. In contrast, the charcoal contains a mixed composition of carbonaceous material and mineral ash components, resulting in a multifunctional surface comprising aromatic carbon structures, oxygenated groups, and inorganic phases.

These compositional differences directly influence adsorption behavior. The silica adsorbent favors metal uptake through surface complexation and ion exchange at silanol sites, while the charcoal provides multiple binding

mechanisms, including electrostatic attraction, π–metal interactions, and coordination with oxygen-containing functional groups. The presence of mineral-derived elements in the charcoal further enhances surface heterogeneity, which can promote diffusion-controlled adsorption and higher metal retention.

The SEM and EDX analyses corroborate the FTIR findings and adsorption results, confirming that both adsorbents possess structurally and chemically favorable characteristics for heavy metal removal. However, the distinct morphological and compositional features of activated silica and corn cob charcoal explain their differing adsorption affinities and kinetic behaviors toward Pb(II) ions.

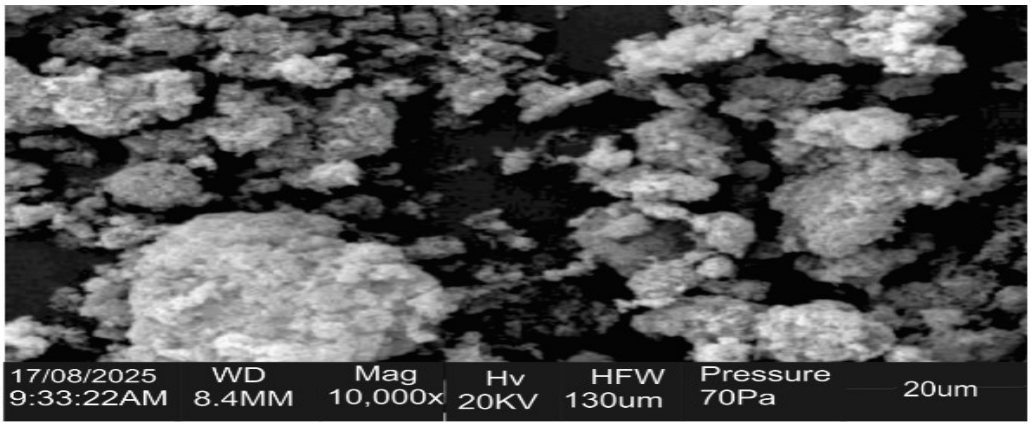

Fig. 5a: The SEM micrograph of activated silica

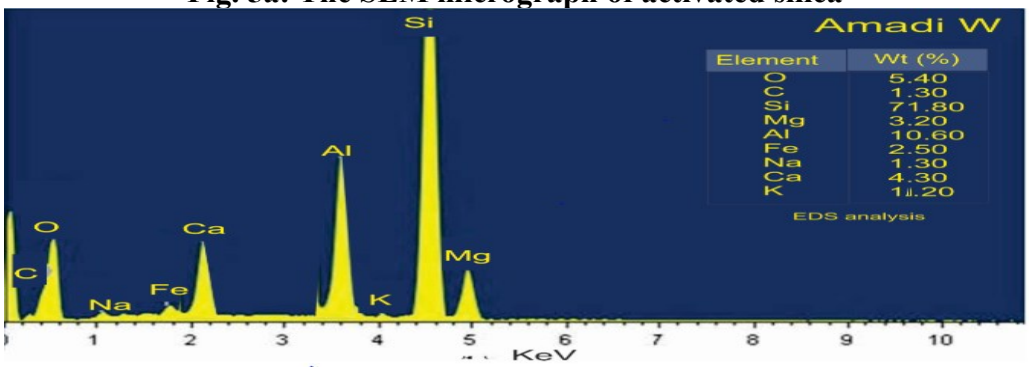

Fig. 5b: Fig 5b: The EDS of activated silica

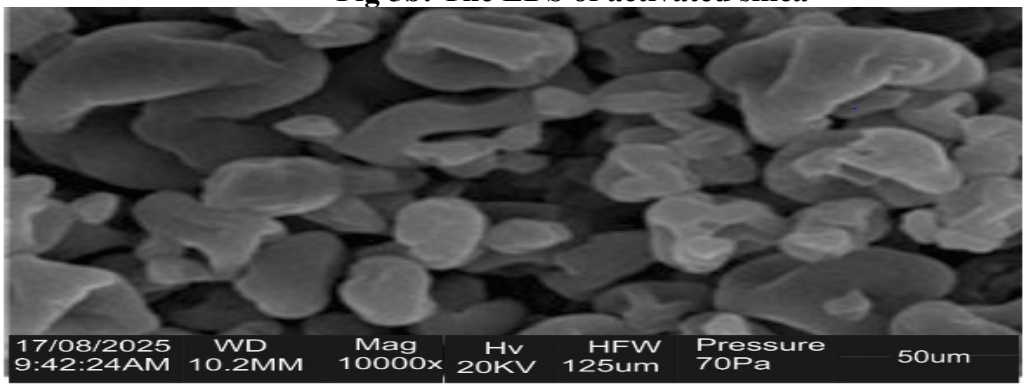

Fig. 6a The SEM micrograph of charcoal

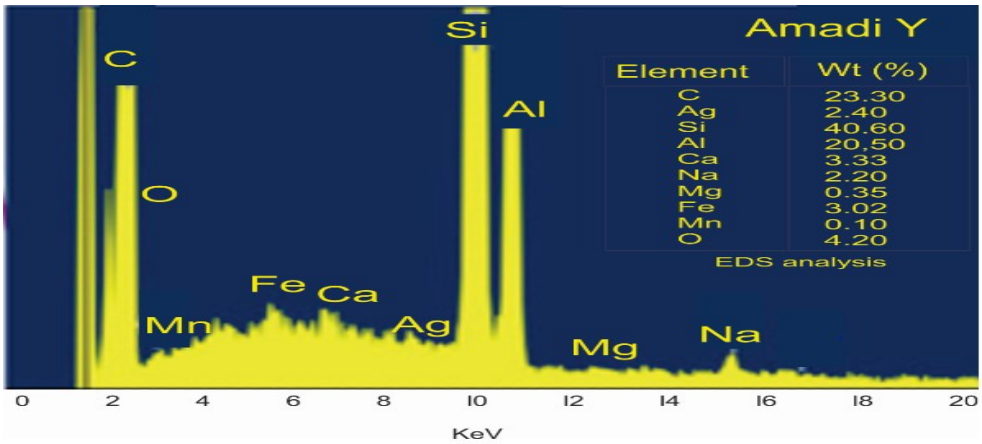

Fig.6b: The EDX of charcoal

The SEM micrograph of activated silica reveals agglomerated fine particles with rough and highly porous surfaces. These morphological features enhance surface exposure of silanol (–Si–OH) and siloxane (–Si–O–Si–) groups previously identified in the FTIR spectra at 3462, 1055, and 977 cm^{-1}. The high density of exposed silanol groups, confirmed by FTIR, coupled with the rough and porous morphology observed in SEM, facilitates rapid diffusion of Pb(II) ions to active sites and promotes surface complexation. This structural–functional synergy explains the strong FTIR peak shifts and intensity reductions observed after Pb(II) adsorption, particularly at the Si–O–Si asymmetric stretching band (≈1055 cm^{-1}), indicating metal–silicate bond formation.

In contrast, the SEM image of the activated charcoal shows a heterogeneous pore structure with well-developed cavities formed during carbonization. These pores expose aromatic carbon frameworks and oxygen-containing functional groups identified in the FTIR spectra, such as aromatic C=C stretching (1561 cm^{-1}), phenolic groups (1364 cm^{-1}), and aromatic C–H out-of-plane bending (764 cm^{-1}). The FTIR peak shifts and partial disappearance of these bands after Pb(II) adsorption are consistent with the SEM-observed pore architecture, which allows Pb(II) ions to penetrate the carbon matrix and interact with internal functional sites.

EDX analysis further supports the FTIR findings by confirming the elemental composition of the adsorbents. Activated silica is dominated by silicon and oxygen, validating the FTIR-identified silanol and siloxane groups as the principal adsorption sites. Minor elements such as Al, Ca, and Mg detected by EDX may contribute additional electrostatic interactions, but FTIR evidence indicates that Pb(II) binding is primarily associated with Si–O functionalities.

For the charcoal, EDX reveals a carbon-rich matrix with significant oxygen and mineral ash components, including silicon and aluminium. This mixed composition corroborates the FTIR detection of both carbonaceous and inorganic functional groups. The coexistence of aromatic structures and mineral phases enhances surface heterogeneity, allowing Pb(II) ions to bind through multiple mechanisms, including coordination with oxygenated groups and interaction with aromatic carbon sites.

The SEM-observed pore characteristics of both adsorbents provide a mechanistic explanation for their kinetic behavior. The relatively uniform, fine pores and high external surface area of activated silica favor rapid initial adsorption controlled by surface reactions. This morphological feature is consistent with kinetic models that emphasize chemisorption processes, such as the pseudo-second-order model, which assumes that adsorption rate is governed by the availability of active sites and

electron-sharing interactions, as supported by FTIR-identified metal–oxygen bonding.

Conversely, the charcoal's broader and more heterogeneous pore network promotes intraparticle diffusion and multilayer adsorption. The presence of larger pores and internal cavities observed in SEM suggests that diffusion into the carbon matrix plays a significant role, particularly at later adsorption stages. This structural behavior aligns with kinetic outcomes typically described by intraparticle diffusion or mixed-control models, where both surface adsorption and pore diffusion influence the overall rate. The FTIR-observed involvement of aromatic and phenolic groups further supports a combination of physical adsorption and chemical interactions.

Overall, the integration of SEM/EDX and FTIR analyses confirms that adsorption efficiency and kinetics are governed by the interplay between surface chemistry and pore structure. Activated silica exhibits adsorption dominated by surface complexation at silanol sites, facilitated by fine pores and high surface accessibility, leading to faster kinetics. In contrast, the corn cob charcoal demonstrates adsorption controlled by both surface functional groups and pore diffusion, resulting in comparatively slower but potentially higher-capacity adsorption.

This multi-technique correlation provides strong mechanistic evidence that the observed kinetic behaviors are a direct consequence of the structural and chemical properties of the adsorbents, thereby validating their effectiveness for Pb(II) removal from wastewater.

3.2. Studying the optimal conditions for adsorption of lead, nickel and cadmium

3.2.1 Effect of pH on the adsorption of the metal ions

The adsorption behavior of Pb(II), Cd(II) and Ni(II) ions on the two prepared adsorbents, viz. pure silica and charcoal were investigated with respect to pH, and the findings are presented in Figs. 7 and 8. The variation of pH was recorded in the pH range of 2–10 In case of silica and charcoal, the removal of Pb(II), Cd(II) and Ni(II) ions was found to be increasing with an increase in pH from 2 to 4 for Pb(II) ions but increased to 6 for both Cd(II) and Ni(II) ions, after which the removal was found to be in decreasing order up to 10.

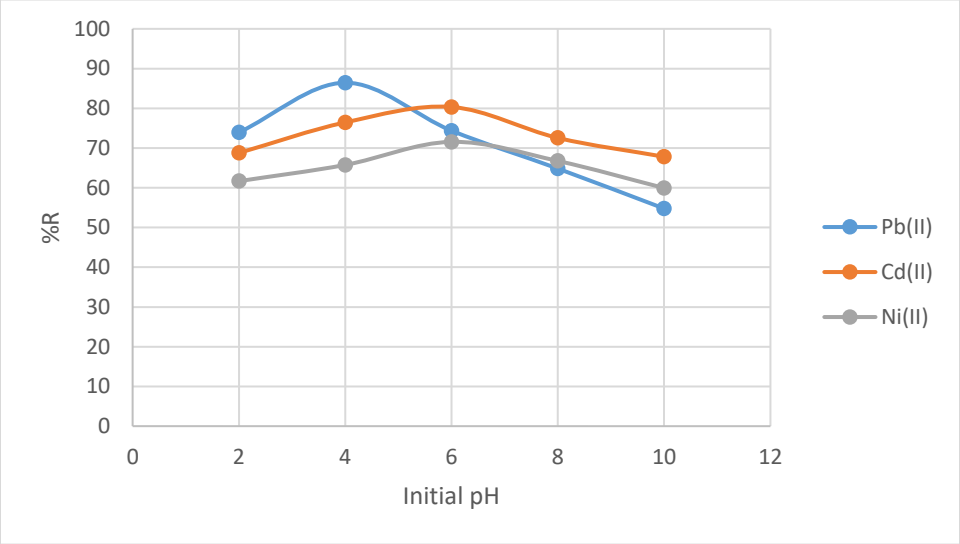

Fig 7: Variation of %R with pH for the absorption of metal ions onto pure silica at initial concentration of 30mg/L for each metal ions at 303K

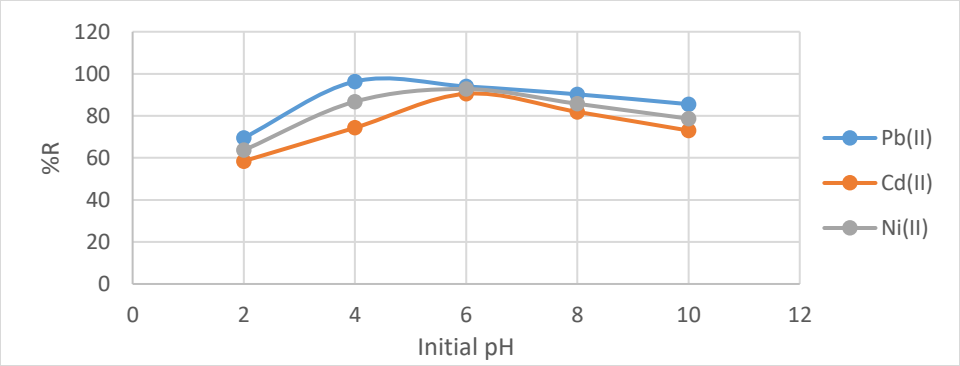

Fig 8: Variation of %R with pH for the absorption of metal ions onto charcoal at initial concentration of 30 mg/L for each metal ions at 303 K

Below pH 4 for Pb(II), for lead and 6 for Cd(II) and Ni(II) ions, the proton concentration predominates and strongly repels the positively charged adsorbates, resulting in the lowest metal ions percentage removal observed for Pb(II), Cd(II) and Ni(II) ions. The presence of functional groups plays a vital role in enhancing the adsorption through electrostatic attraction (Igwegbe *et al*., 2021; Azzam *et al*., 2022). The highest removal efficiency at pH 4 for Pb and pH 6 for Cd and Ni were found to be 96.34, 90.49 and 92.75%, in the case of charcoal, but were 86.94%, 80.34% and 71.56% for pure silica, respectively, when used at 4.0gL^{-1} of adsorbent dose for 60 min under room temperature conditions. Similar kinds of optimization were found by the earlier studies with different adsorbents (Ma *et al*., 2015; Azzam *et al*., 2022). This optimized pH value (viz. pH 4 for Pb but pH 6 for both Cd and Ni) were maintained for further experiments using the two adsorbents. (Ersan *et al*., 2023; Jorge *et al*., 2024).

3.2.2. Effect of temperature on the adsorption process

The influence of temperature on the equilibrium adsorption capacity for the metal ions by the two adsorbents was determined at temperatures ranging from 30 to 70 °C, with initial metal ion concentration of 30 mg/L and pH 6 for Cd(II) and Ni(II) ions and pH 4 for Pb(II) ions are presented in Figs. 9 and 10. The results obtained suggest that adsorption of the metal ions from their solutions increased with increase in temperature, reaching a maximum at 40° C for their adsorption onto the silica and charcoal and afterward decreased as the temperature was increased above this temperature, as shown in Figs. 9 and 10. It had been stated that physisorption usually decreases with an increase in temperature, while chemisorption increases as the temperature is increased (Eddy *et* al., 2008) . This suggests that the bonding of the metal ions to the adsorbents in our study could have involved a combination of chemical interaction and physical adsorption. At the optimum temperatures for sorption of lead(II), cadmium(II) and Nikel(II) ions onto the adsorbents, the pores of the adsorbents may have been enlarged, resulting in an increase in the surface area available for adsorption, diffusion and penetration of the metal ions within the pores of the adsorbents and thereby causing an increase in adsorption. Also, increasing the temperature is known to increase the diffusion rate of adsorbate molecules within the pores as a result of decreasing solution viscosity, and this will in turn alter the equilibrium capacity of the adsorbents for the metal ions. The decrease in the amounts of metal ions adsorbed with increasing temperature above 40° C respectively for adsorption of the metal ions onto the silica and charcoal could have resulted from any of the following: (i) deactivation of the adsorbent surfaces or destruction of some active sites on

the adsorbent phases due to weakening of the bonds (Mohamed *et al*., 2024) (ii) increase in the relative escaping tendency (desorption) of the metal ions from the adsorbent phase to the bulk phase resulting from weakening of attractive forces between the active sites of the sorbents and the metal ions and also between the adjacent molecules of the adsorbed phases (Amadi *et al*., 2019). This weakening of attractive forces may have caused the metal ions to detach from the adsorbent surfaces into the solution phase.

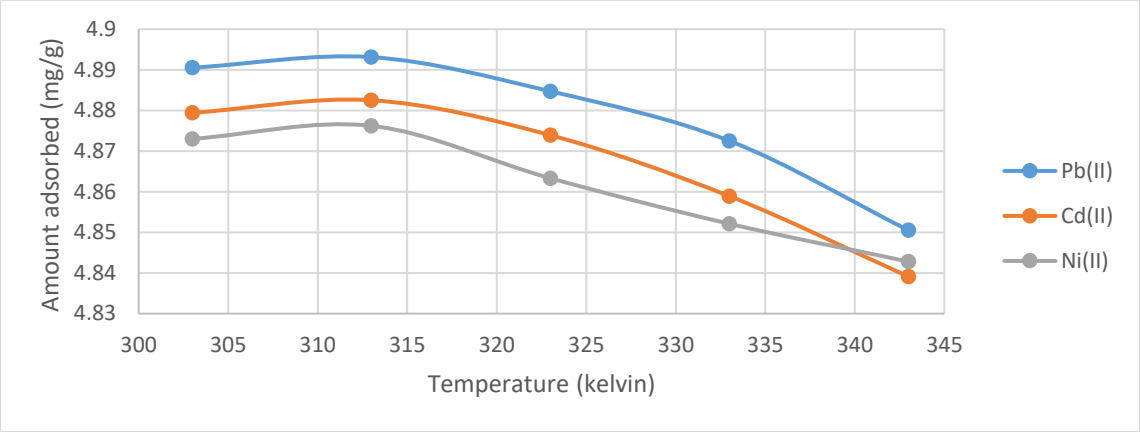

Fig. 9: Plot of sorption capacity (qe) vs temperature for the adsorption of the metal ions onto silica

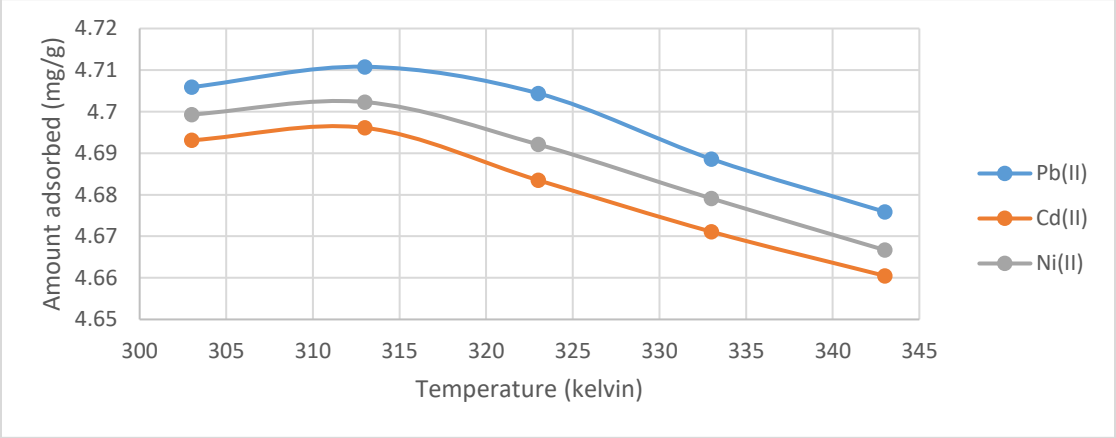

Fig. 10: Plot of sorption capacity (qe) vs temperature for the adsorption of the metal ions onto charcoal

3.2.3 Effect of Contact Time

The amount of metal ion adsorbed by an adsorbent at a particular time is one of the important factors that characterize the efficiency of an adsorption system. Results indicate that adsorption increases with an increase in contact time before equilibrium is attained, as shown in Figs. 11 and 12. Other parameters such as adsorbent mass, pH of solution, temperature and concentration of the metal ions were kept constant. Optimum contact time for adsorption of Pb(II), Cd(II), and Ni(II) ions by 0.1 g of the two adsorbents was 120 min. The figures indicate that a greater amount of Pb(II), Cd(II) and Ni(II) ions were adsorbed by both silica and charcoal within the first 80 min. After that, there was about 80 % levelling effect, indicating attainment of equilibrium for the adsorption process. In general, the pure silica adsorbent showed higher removal of the Pb(II), Cd(II) and N(II) ions compared to those adsorbed onto charcoal.

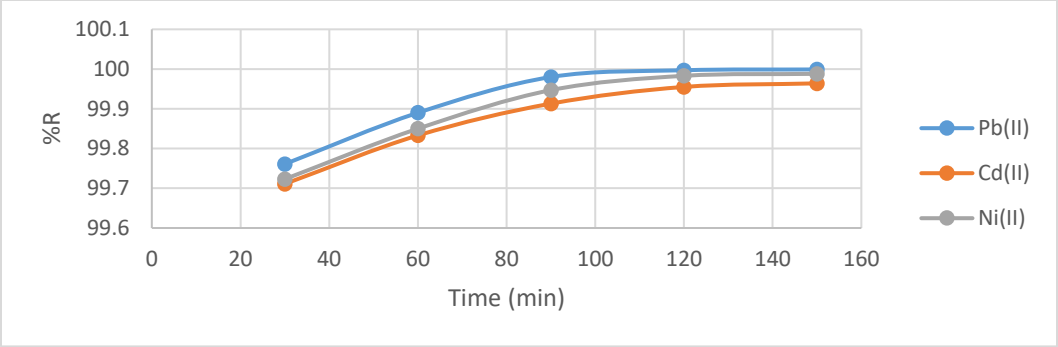

Fig. 11: Effect of contact time on the adsorption of metal ions onto biochar

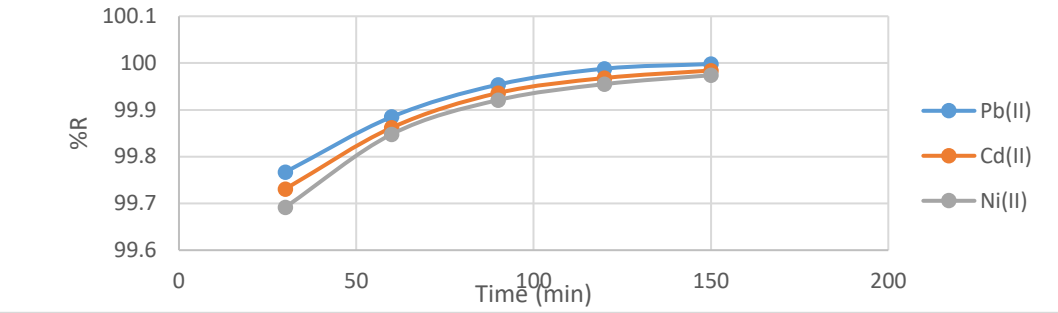

Fig. 12: Effect of contact time on the adsorption of metal ions onto silica

3.3 Kinetic Model

Adsorption kinetics is an effective method of evaluating the rate and mechanism of adsorption of metal ions onto adsorbents. In the present study, three different adsorption kinetic models viz; pseudo first-order, pseudo second-order and the intra-particle diffusion models, were applied to analyze the experimental data. The conformity between the experimental data and the model-predicted values was expressed by the correlation coefficients (R^2 values close or equal to 1). A relatively high R^2 value indicates that the model successfully describes the kinetics of the metal ion adsorption.

3.3.1 The pseudo first-order model

The integrated pseudo first-order equation is generally given as equation 2 (Huang *et al*., 20117; Ogoko *et al*., 2023):

$$\log(qe-qt) = \log(qe) - \frac{k_1}{2.303}(t) \qquad (2)$$

where q_e and q_t are the adsorption capacities (mg/g) at equilibrium and at a time t, respectively, k_1 is the pseudo-first-order rate constant (min^{-1}). The plots of log (q_e - q_t) versus t were linear, from which k_1 values for the metal ions were determined from the slope of the linear plots and are presented in Table 1. Figs. 13 and14 show the linear plots for the pseudo-first-order model.

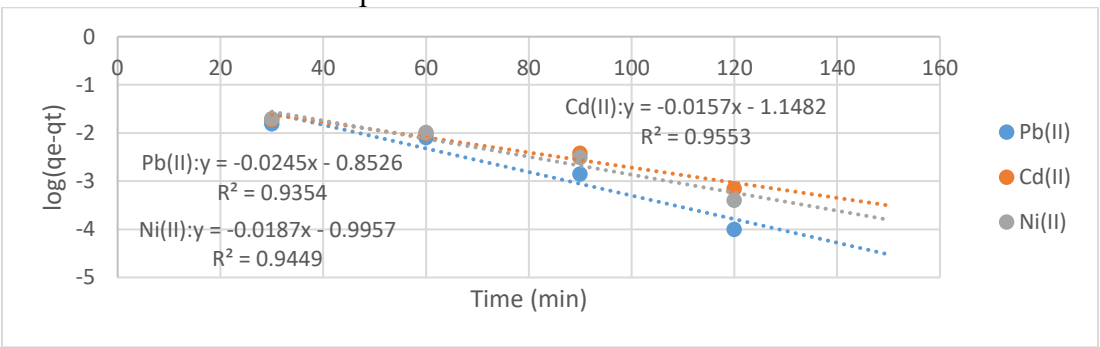

Fig. 13: Pseudo-first order plot of log(qe-qt) vs t for adsorption of the metal ions onto charcoal

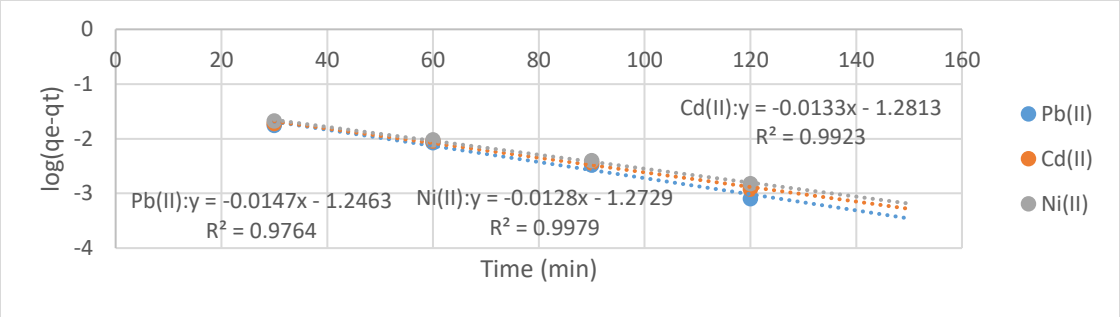

Fig 14: Pseudo-first order plot of log(qe-qt) vs t for adsorption of the metal ions onto pure silica

Table 1: Kinetic parameters for pseudo-first-order reaction at 30 ^{0}C

	Pure Silica			Charcoal		
	Pb(II)	**Cd(II)**	**Ni(II)**	**Pb(II)**	**Cd(II)**	**Ni(II)**
qe cal (mg/g)	0.0567	0.0523	0.0533	0.1404	0.0711	0.101
Qe(expt)(mg/g)	7.4999	7.4988	7.4981	7.4999	7.4973	7.4991
k_1 (min^{-1})	0.0339	0.0306	0.0295	0.0564	0.0362	0.0431
R^2	0.9764	0.9923	0.9979	0.9354	0.9553	0.9449

3.3.2 Pseudo-Second Order Model

The pseudo-second order adsorption kinetic rate equation is expressed as (Legergren, 1898):

$$\frac{dqt}{dt} = k_2(qe - qt)_2 \quad (3)$$

where k_2 (g/mg/min) is the rate constant of pseudo-second order adsorption, qe and qt (mg/g) are the sorption capacity at equilibrium time and at time t, respectively. For the boundary conditions t = 0 to t = t and qt = qt, the integrated form of the above equation becomes:

$$\frac{t}{qt} = \frac{1}{ho} + \frac{1}{qe}(t) \quad (4)$$

where $h_o = k_2qe^2$ is usually described as the initial adsorption rate as t approaches zero. The pseudo-second-order model was applied in this analysis and a plot of t/qt vs t gave linear plots, which allowed the evaluation of qe, k_2 and ho. As shown in Table 2 and Figs. 15 and 16, the experimental adsorption data fitted the pseudo-second-order model perfectly as observed by the high correlation coefficients (R^2 =1). The pseudo-second-order parameters for the adsorption of the metal ions are presented in Table 1. These parameters were calculated from the intercept and slope of the linear plots of t/qt versus t. The equilibrium adsorption capacities, q_e calculated from the pseudo-second-order kinetic model, agree very closely with the experimental values. The fitting of the experimental adsorption data into pseudo second-order model shows that the rate of occupation of active sites is proportional to the square of the number of unoccupied sites (Amaku *et al*., 2025). Pseudo-first-order and pseudo-second-order theoretical fitting parameters are listed in Tables 1 and 2, respectively. Results showed that the calculated amounts of metal adsorbed ($q_{e,cal}$) by the pseudo-first-order model differ substantially from those measured experimentally, whereas those obtained from the pseudo-second-order kinetic model are very close to experimental data despite high correlation coefficient values, suggesting that the adsorbent systems can be well described by the pseudo-second-order kinetic model (Lee & Choi, 2018; Alwared & Sadiq, 2019)

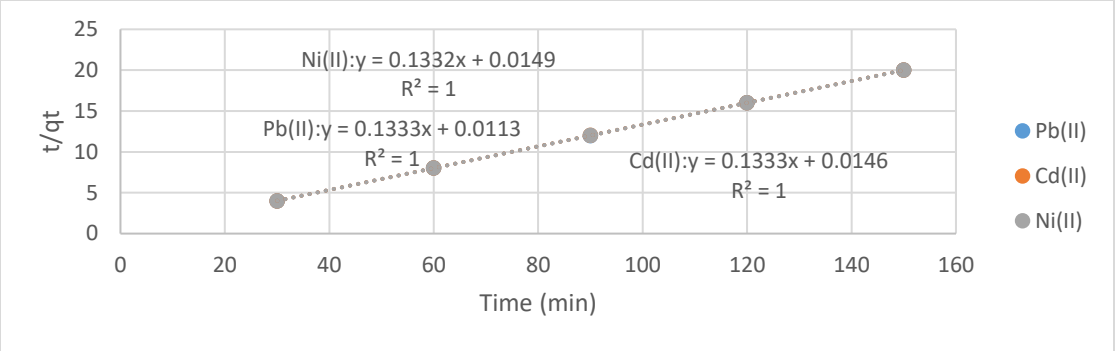

Fig. 15: Pseudo-second order plot of t/qt vs t for adsorption of the metal ions onto charcoals

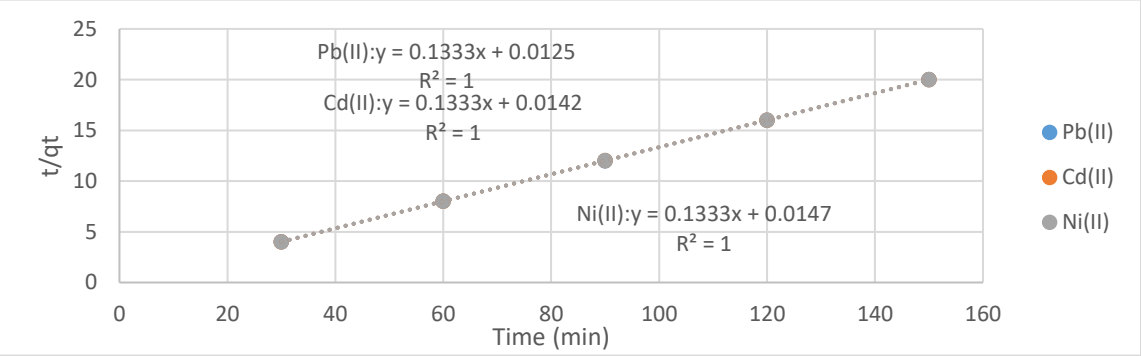

Fig. 16: Pseudo-second order plot of t/qt vs t for adsorption of the metal ions onto pure silica

Table 2. Pseudo-second-order kinetic parameters at 30 °C

onstant	Pure Silica			Charcoal		
	Pb(II)	Cd(II)	Ni(II)	Pb(II)	Cd(II)	Ni(II)
qe cal(mg/g)	7.5019	7.5019	7.5019	7.5019	7.5018	7.5075
qe expt (mg/g)	7.4999	7.4988	7.4981	7.4999	7.4973	7.4991
k_2(g/mg^{1}min^{-1})	1.4215	1.2513	1.2087	1.5725	1.2171	1.1908
ho(mg/g/min)	80.0000	70.4225	68.0227	88.4956	68.4932	67.1141
R^2	1.0000	1.0000	1.0000	1.0000	1.0000	1.0000

3.3.3 Elovich model

Elovich equation is also used successfully to describe second order kinetic assuming that the actual solid surfaces are energetically heterogeneous, but the equation does not propose any definite mechanism for adsorbate–adsorbent (Zhang & Stanforth, 2005). It has been extensively accepted that the chemisorption process can be described by this semi-empirical equation (Low 1960; Gupta *et al*., 2019). The Elovich equation, developed for describing the kinetics of heterogeneous chemisorptions, assumes a heterogeneous distribution of adsorption (which defines heterogeneousity) or activation energies that vary continuously with surface coverage, and it's widely used in liquid-solid. The Elovich or Roginsky–Zeldovich equation is generally expressed according to equation 5 (Akpanudo & Olabemiwo, 2024a,b)

$$\frac{dqt}{dt} = \alpha \exp^{(-\beta qt)} \qquad (5)$$

Where, α is the initial adsorption rate (mg/g/min), β is the desorption constant

(g/mg). If the adsorption fits the Elovich model, a plot (Figs 17 and 18) of qt versus ln (t) should give a linear relationship with a slope of (1/β) and an intercept of 1/β In (αβ). In other words, the parameter α represents the rate of chemisorptions, and the parameter β is related to the extent of surface coverage and the activation energy of chemisorptions. To simplify the Elovich (equations 5), (Renugadevi *et al*., 2011) assumed αβ ≫ 1 and applying the boundary conditions qt=0 at t=0 and qt=qt at t = t, equation 5 becomes:

$$qt = \frac{1}{\beta} In\ (\alpha\beta) + \frac{1}{\beta} In(t) \qquad (6)$$

The coefficients of correlation (R^2 values) were all high for the two adsorbents, indicating that the model adequately described the experimental data.

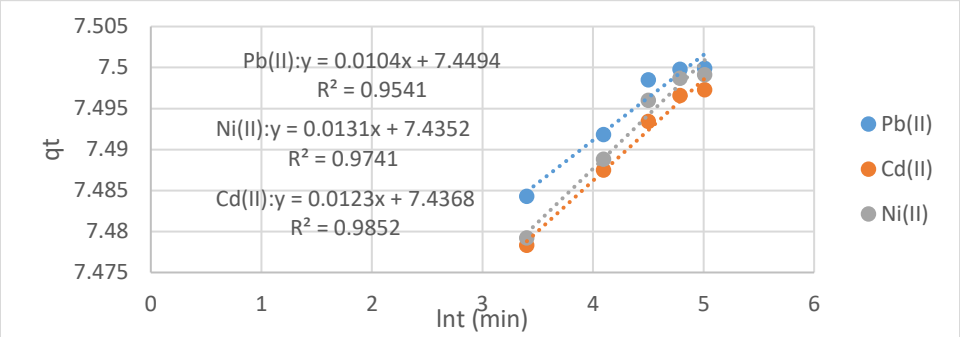

Fig..17: Elovich plot for the Adsorption of metal ions onto charcoals

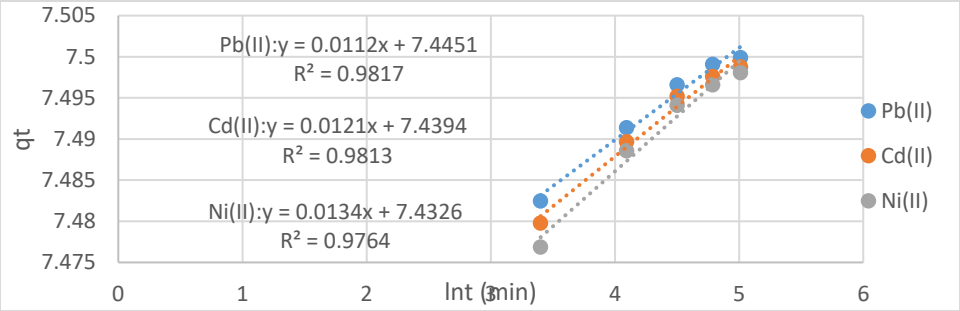

Fig. 18: Elovich plot for the Adsorption of metal ions onto pure silica

Table 3: Elovich model parameters for the adsorption of metal ions onto charcoals and pure silica

Constant	Pure Silica			Charcoal		
	Pb(II)	Cd(II)	Ni(II)	Pb(II)	Cd(II)	Ni(II)
B	89.2857	82.6446	74.6269	96.1538	81.3008	76.3359
A	20.2379	20.2224	20.2039	20.2496	20.2153	20.2109
R^2	0.9394	0.9374	0.9277	0.9064	0.9489	0.9327

3.4 Intraparticle diffusion models

The transport mechanism of adsorption could be either film-diffusion controlled or particle diffusion controlled. Adsorption of solute particles involves the following diffusion processes: the diffusion of the adsorbates (metal ions) through the bulk of the solution to the film surrounding the adsorbents, and then into the micropores and macropores of the adsorbents. Several models have been proposed for studying the mechanism of adsorption processes by intraparticle diffusivity, including those presented below.

3.4.1 McKay & Poots model

This model equation as developed by McKay and Poots states that the amount of solutes adsorbed can be expressed in terms of the square root of time and is expressed as: Alshammari *et al*., 2025).

$$qt = Xi + kit^{1/2} \quad (7)$$

Where Xi is the boundary layer diffusion effects (mg/g), Ki is the intraparticle diffusion rate constant (mg/g $min^{0.5}$). The plots of the amount of metal ions adsorbed, qt, against the square root of time, $t_{1/2}$ for the adsorption process are shown in Figs. 19 and 20. The slope of the linear plots gives the initial rate of sorption controlled by intraparticle diffusion, K′ (mg $g^{-1}min^{-0.5}$) while the extrapolation of the linear plots to the time axis gives the intercepts of the plots, Xi (mg/g) which is proportional to the boundary layer thickness. The intraparticle diffusivity parameters and the correlation coefficients (R^2 values) are presented in Table 4. The high values of X_i i.e. boundary layer thickness, depict higher adsorption capacities. The boundary layer gives an insight into the tendency of the metal ions to adsorb to the adsorbent phase or remain in solution. Since diffusion takes place, the boundary layer is viewed as a viscous drag existing between the adsorbent surfaces and the metal ion solutions diffusing across its surface. As shown in Table .4, the boundary layer thickness varied from 7.4623 to 7.4727 mg/g, which is an indication of high adsorption capacity of the metal ions by the adsorbents. Generally, it could be seen that the model to a good approximation, fits the experimental adsorption data as observed from the high R^2 values, which ranged from 0.9064 to 0.9489 and also confirms that the sorption process may be intraparticle diffusion controlled (Gao *et al*., 2017).

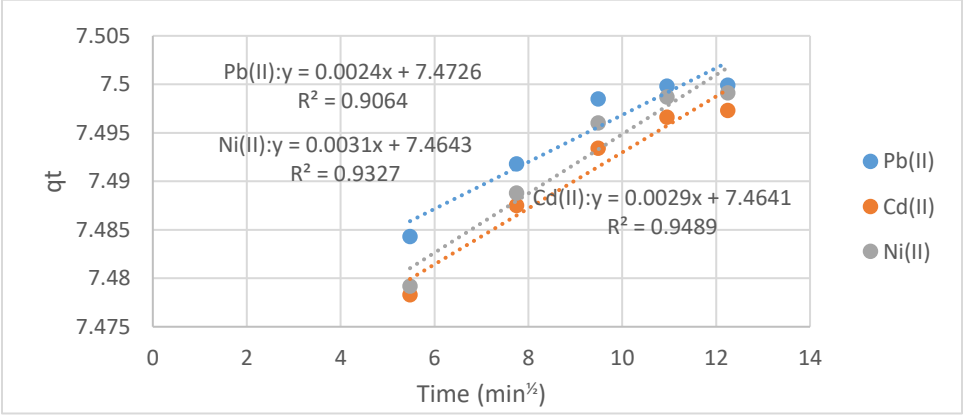

Fig. 19: McKay and poot intra particle Diffusion Model for the Adsorption of Pb(II), Cd(II) and Ni(II) ions onto charcoals

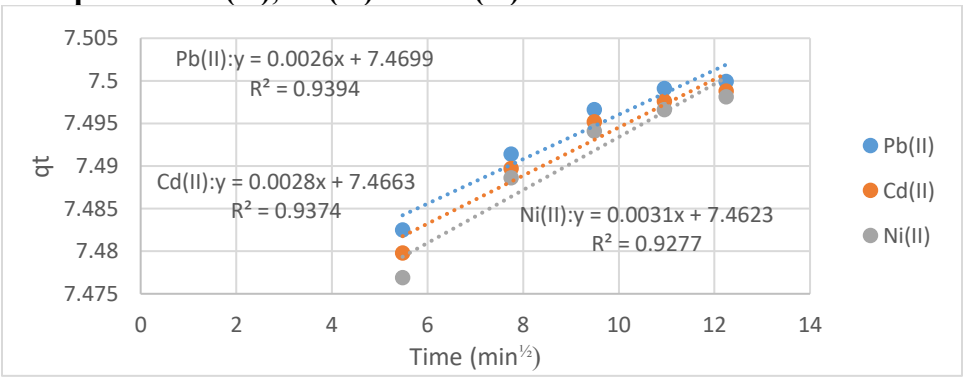

Fig. 20: McKay and poot intra particle Diffusion Model for the Adsorption of Pb(II), Cd(II) and Ni(II) ions onto pure silica.

Table 4: Adsorption parameter based on McKay and Intra particle Diffusivity Models for Pb(II), Cd(II) and Ni(II) ions adsorption onto charcoal and pure silica

Constant	Pure Silica			Charcoal		
	Pb(II)	Cd(II)	Ni(II)	Pb(II)	Cd(II)	Ni(II)
Xi	7.4699	7.4663	7.4623	7.4726	7.4641	7.4643
K_{id}(mg/g $min^{0.5}$)	0.0026	0.0028	0.0031	0.0024	0.0029	0.0031
R^2	0.9394	0.9374	0.9277	0.9064	0.9489	0.9327

4.0 Conclusion

The study indicated that the adsorption behavior of Pb(II), Cd(II), and Ni(II) ions onto pure silica and charcoal can be further explained by the physicochemical properties of the adsorbents revealed from FTIR, SEM, and EDX analyses. FTIR spectra indicated the presence of key functional groups such as –OH, –Si–O–Si–, –C=O, and –COOH on the adsorbent surfaces, which are known to enhance metal ion binding through electrostatic attraction, complexation, and hydrogen bonding (Igwegbe *et al*., 2021; Azzam *et al*., 2022). The intensity of these functional groups suggests a higher density of active sites on charcoal compared to silica, which correlates with the higher adsorption efficiencies observed for Pb(II), Cd(II), and Ni(II) ions on charcoal at the optimal pH and contact time.

SEM images of both adsorbents revealed porous and rough surface morphologies, which provide a high surface area for adsorption. Charcoal exhibited a more heterogeneous and highly porous surface compared to silica, facilitating greater diffusion and penetration of metal ions into the adsorbent matrix. This supports the observed kinetics, where rapid adsorption occurred within the first 80 min, followed by equilibrium, consistent with the multilayer adsorption and the presence of heterogeneous active sites as described by the Elovich model.

EDX analysis confirmed the presence of adsorbed Pb, Cd, and Ni ions on both adsorbents after the adsorption process. The EDX spectra showed strong signals corresponding to the respective metal ions, providing direct evidence of successful uptake. The relative intensities of these peaks were higher for charcoal, further corroborating the superior adsorption capacity of charcoal compared to silica.

The combined FTIR, SEM, and EDX results provide a mechanistic insight into the adsorption process: (i) the functional groups identified by FTIR act as binding sites for metal ions through electrostatic and chemical interactions, (ii) the porous and rough structure observed via SEM facilitates diffusion and accessibility of the ions to active sites, and (iii) the actual accumulation of metal ions on the adsorbents, evidenced by EDX, confirms the efficiency and capacity of the adsorbent surfaces. These structural and compositional characteristics explain the pH-, temperature-, and time-dependent adsorption behavior observed in the present study, supporting the conclusions drawn from kinetic and intraparticle diffusion analyses.

5.0 References

Abdel-Salam, M., Abuzaid, A., Mouhmoud, F., & Abbas, M. (2025). Increasing maize productivity in arid sandy soils using combinations of (normal/acidified) biochar

and elemental sulfur. *Egyptian Journal of Soil Science*, 65(1). https://doi.org/10.21608/ejss.2024.328587.1887

Abuzaid, A., Abdel-Salam, M., Abbas, M., Khalil, F., & Abdelhafez, A. (2025). Effectiveness of biochar and elemental sulfur for sustaining maize production in arid soils. *Egyptian Journal of Soil Science*, 65(1), pp. 163–177. https://doi.org/10.21608/ejss.2024.324620.1875

Ai, L., Zhang, C., Liao, F., Wang, Y., Li, M., Meng, L., & Jiang, J. (2011). Removal of methylene blue from aqueous solution with magnetite loaded multi-wall carbon nanotube: kinetic, isotherm and mechanism analysis. *Journal of hazardous materials,* 198, pp. 282-290.

Akpanudo, N. W., & Chibuzo, O. U. (2020). *Musanga cecropioides* sawdust as an adsorbent for the removal of methylene blue from aqueous solution. *Communication in Physical Sciences,* 5, 3, pp. 362–370.

Akpanudo, N. W., & Olabemiwo, O. M. (2024a). Green synthesis and characterization of copper nanoparticles (CuNPs) and composites (CuC) using the *Echinochloa pyramidalis* extract and their application in the remediation of PAHs in water. *Water Practice and Technology,* 19, 2, pp. 324–342. https://doi.org/10.2166 /wpt.2024.011

Akpanudo, N. W., & Olabemiwo, O. M. (2024b). Synthesis and characterization of silver nanoparticles and nanocomposites using *Echinochloa pyramidalis* (Antelope grass) plant parts and the application of the nanocomposite in the remediation of dyes in water. *South African Journal of Chemical Engineering,* 47, 1, pp. 98–110. https://doi.org/10.1016/j.sajce.2023.11.008

Alshammari, N. A. H., Elsayed, N. H., Alatawi, R. A. S., Bukhari, A. A. H., Alnawmasi, J. S., Alshareef, S. A., Alnahdi, K. M., Alhawiti, A. S. & El-Binadary, A. A. (2025). Synthesis of pomegranate peel-activated carbon encapsulated onto carboxymethylcellulose and polyethylenimine for cadmium (II) adsorption: optimization, kinetics and isotherm modeling, *Int. J. Biol. Macromol.* 310, 143348, https://doi.org/10.1016/j.ijbiomac.2025.143348

Alwared, A. I., & Sadiq, N. A. (2019). Competitive removal of lead copper and cadmium ions by sorptive flotation using marble wastes. *International Journal of Environment and Waste Management*, 23, 2, , pp. 156-178.

Amadi, O. K., Ekuma, F. K., Okoro I. A. & Aleruchi C. C. (2019). Kinetics studies of sorption of Pb(II), Cd(II) and Ni(II) ions from aqueous solution using functionalized calopo (*Calopogonus mucunoides*) seed pod. *J. Chem Soc. Nigeria*, 44, 6, pp. 1183 -1190

Amaku, J. F., Amadi, O. K., Mtunzi, F. M. & Greener, J. (2025). Facile synthesis of ZnONP/carbon-coated-eggshell nanocomposite: fast and efficient adsorbents for amoxicillin sequestration, *Chemical Papers*. https://doi.org/10.1007/s11696-025-04148-8

Awaka-Ama, J. J., Udo, G. J., Uwanta, E. J., Etukudo, N. J., Akpanudo, N. W., & Igwe, R. (2024). Comparative analysis of heavy metal contamination in regular and artisanal petroleum products in Akwa Ibom State, South-South Nigeria. *Communication in Physical Sciences*, 11, 3, pp. 559–568.

Azzam, A.B., Tokhy, Y.A., Farida, M., & Younes, A.A. (2022). Construction of porous biochar decorated with NiS for the removal of ciprofloxacin antibiotic from pharmaceutical wastewaters. *J. Water Process Eng.* 49, 103006. https://doi.org/10.1016/j.jwpe.2022.103006

Batheja, K., Sinha, A., & Seth, G. (2009). Studies on water treatment for removal of nitrate. *Asian J. Exp. Sci,* 23, 1, pp. 61-66.

Bedemo, A., Chandravanshi, B. S., & Zewge, F. (2016). Removal of trivalent chromium from aqueous solution using aluminum oxide hydroxide. *SpringerPlus*, 5, pp. 1-11.

Bilal, M., Ihsanullah, I., Younas, M., & Shah, M. U. H. (2021). Recent advances in

applications of low-cost adsorbents for the removal of heavy metals from water: A critical review. *Separation and purification technology,* 278, 119510. https://doi.org/10.1016/j.seppur.2021.119510

Chakraborty, R., Asthana, A., Singh, A. K., Jain, B., & Susan, A. B. H. (2022). Adsorption of heavy metal ions by various low-cost adsorbents: a review. *International Journal of Environmental Analytical Chemistry,* 102, 2, , pp. 342-379.

Chronopoulos, J., Haidouti, C., Chronopoulou-Sereli, A., & Massas, I. (1997). Variations in plant and soil lead and cadmium content in urban parks in Athens, Greece. *Science of the total environment,* 196, 1, , pp. 91-98.

Deng, L., Su, Y., Su, H., Wang, X., & Zhu, X., (2007). Sorption and Desorption of Lead (II) from Wastewater by Green Algae (*Cladophora fascicularis*), *J. Hazar. Mater.* 143: pp. 220-225,

Diagomanolin, V., Farhang, M., Ghazi-Khansari, M., and Jafarzadeh, N. (2004). Heavy metals (Ni, Cr, Cu) in the Karoon River, Iran. Toxicology letters, 15, 1, pp. 63-67.

Donia, A. M., Atia, A. A., Al-amrani, W. A.& El-Nahas, A. M. (2009). Effect of structural properties of acid dyeson their adsorption behaviour from aqueous solutions by amine modified silica, *J. Hazard. Mater.,* 161, pp. 1544-1550.

Dureja, H.,& Madan, A. (2007). Adsorption in pharmacy: A review. *Drug Delivery Technology,* 7, 8, pp. 58-64.

Eddy, N. O., Garg, R., Ukpe, R. A., Akpanudo, N. W., Abugu, H., Garg, R., Anjum, A., & Anand, B. (2024a). Ethical and environmental implications associated with the application of nanoparticles. In *Smart and Sustainable Applications of Nanocomposites* (pp. 274–299). https://doi.org/10.4018/979-8-3693-1094-6.ch010

Eddy, N. O., Garg, R., Ukpe, R. A., Akpanudo, N. W., Abugu, H., Garg, R., Anjum, A., & Galadanci, S. (2024). Ethical and environmental implications associated with the application of nanotechnology. In *Smart and Sustainable Applications of Nanocomposites* (pp. 274–299).

Eddy, N. O., Garg, R., Ukpe, R. A., Ameh, P. O., Gar, R., Musa, R., Kwanchi, D., Wabaidur, S. M., Afta, S., Ogbodo, R., Aikoye, A. O., & Siddiqui, M. (2024d). Application of periwinkle shell for the synthesis of calcium oxide nanoparticles and in the remediation of Pb^{2+}-contaminated water. *Biomass Conversion and Biorefinery.* https://doi.org/10.1007/s13399-024-05285-y

Eddy, N. O., Jibrin, J. I., Ukpe, R. A., Odiongenyi, A., Iqbal, A., Kasiemobi, A. M., Oladele, J. O., & Runde, M. (2024c). Experimental and theoretical investigations of photolytic and photocatalysed degradations of crystal violet dye (CVD) in water by oyster shell-derived CaO nanoparticles (CaO-NP). *Journal of Hazardous Materials Advances, 13, pp. 100413.* https://doi.org/10.1016/j.hazadv.2024.100413

Eddy, N. O., Odoemelam, S. A., & Akpanudo, N. W. (2008). Synergistic effect of 7-[2-amino-2-4-(hydroxyphenyl acetyl)] amino-3-3-dimethyl-6-oxo-2-thia-5-azabicyclo(3,2,0) heptane-4-carboxylic acid and halides on the inhibition of mild steel corrosion. *Journal of Applied Sciences Research, 4, 12, pp. 1963–1973.*

Eddy, N. O., Oladede, J., Eze, I. S., Garg, R., Garg, R., & Paktin, H. (2024b). Synthesis and characterization of CaO nanoparticles from periwinkle shell for the treatment of tetracycline-contaminated water by adsorption and photocatalyzed degradation. *Results in Engineering, pp. 103374.* https://doi.org/10.1016/j.rineng .2024.103374

Eddy, N. O., Ukpe, R. A., Ameh, P., Ogbodo, R., Garg, R., & Garg, R. (2023c). Theoretical and experimental studies on photocatalytic removal of methylene blue (MetB) from aqueous solution using oyster shell synthesized CaO nanoparticles (CaONPO). *Environmental Science and Pollution Research.* https://doi.org/10. 1007/s11356-022-22747-w

Eddy, N. O., Ukpe, R. A., Garg, R., Garg, R., Odiongenyi, A. O., Ameh, P., & Akpet, I. N. (2023d). Enhancing water purification efficiency through adsorption and

photocatalysis: Models, application and challenges. *International Journal of Environmental Analytical Chemistry.* https://doi.org/10.1080/03067319.2023.2295934.

Ersan, G., Dos Santos, A.J., Lanza, M.R., Perreault, F., & Garcia-Segura, S., 2023. Enhancing the selective ciprofloxacin adsorption in urine matrices through the metal-doping of carbon sorbents. *J. Environ. Manag.* 348, 119298. https://doi.org/10.1016/j.jenvman.2023.119298

Familusi, A. O., ADEKUNLE, A., Badejo, A., & Adeosun, O. J. (2021). Distinctive Features of River Sand, Beach Sand and Granite as Adsorbents in Water and Wastewater Treatment. *The Egyptian International Journal of Engineering Sciences and Technology,* 34, 1, pp. 11 -15.

Gao, X., Yuan, B., Yu, Q., & Brouwers, H. (2017). Characterization and application of municipal solid waste incineration (MSWI) bottom ash and waste granite powder in alkali activated slag. *Journal of Cleaner Production*, 164, pp. 410-419.

Ghazy, S. (1995). Removal of cadmium, lead, mercury, tin, antimony, and arsenic from drinking and seawaters by colloid precipitate flotation. *Separation Science and Technology*, 30, 6, pp. 933-947.

Ghazy, S. E., Gabr, I. M., & Gad, A. H. (2008). Cadmium (II) sorption from water samples by powdered marble wastes. *Chemical Speciation & Bioavailability*, 20, 4, pp. 249-260.

Guesmi, A., Hamadi, N. B., El-Fattah, W. A., Subaihi, A., Alluhaybi, A. A., El- Desouky, M. G., & El-Bindary, A. A. (2025). Efficient removal of pb(II) ions from wastewater via a vanadium metal-organic framework encapsulated with biopolymer carboxymethyl cellulose/polyethylenimine through synthesis, characterization, and box-Behnken optimization, *Int. J. Biol. Macromol.* 318, 145201, https://doi.org/10.1016/ j.ijbiomac.2025.145201

Gupta, S., Sharma, S., Kumar, A. (2019). Biosorption of Ni (II) ions from aqueous solution using modified Aloe barbadensis Miller leaf powder. *Water Science and Engineering,* 12, 1, pp. 27-36.

Hahladakis, J., Smaragdaki, E., Vasilaki, G., & Gidarakos, E. (2013). Use of sediment quality guidelines and pollution indicators for the assessment of heavy metal and PAH contamination in Greek surficial sea and lake sediments. Environmental monitoring and assessment, 185, pp. 2843-2853.

Han, R. P., Zhang, J. H., Zou, W. H., Shi, H. M. & Liu, H. M. (2005). "Equilibrium Biosorption Isotherm for Lead ion on Chaff". *Journal Hazardous Materials B*. 125, pp. 266-271

Huang, J., Yuan, F., Zeng, G., Li, X., Gu, Y., Shi, L., . . . Shi, Y. (2017). Influence of pH on heavy metal speciation and removal from wastewater using micellar-enhanced ultrafiltration. *Chemosphere,* 173, pp. 199-206.

Igwegbe, C.A., Oba, S.N., Aniagor, C.O., Adeniyi, A.G., & Ighalo, J.O., (2021). Adsorption of ciprofloxacin from water: a comprehensive review. *J. Ind. Eng. Chem*. 93, pp. 57–77.

Inyang, M. I., Gao, B., Yao, Y., Xue, Y., Zimmerman, A., Mosa, A., & Cao, X. (2016). A review of charcoal as a low-cost adsorbent for aqueous heavy metal removal. *Critical reviews in environmental science and technology,* 46, 4, pp. 406-433.

Jorge, N.L., Garrafa, M.V., Romero, J.M., Jorge, M.J., Jorge, L.C., Delfino, M.R., Meruvia- Rojas, Y.V., Hern´andez-Laguna, A., & Sainz-Díaz, C.I., (2024). Adsorption of ciprofloxacin on clay minerals in argentinian santa rosa-corrientes soils. *Molecules* 29 (8), 1760.

Lagergren, S. K. (1898). About the theory of so-called adsorption of soluble substances.

Sven. Vetenskapsakad. Handingarl, 24, pp. 1-39.

Lane, T. W., & Morel, F. M. (2000). A biological function for cadmium in marine diatoms. *Proceedings of the National Academy of Sciences,* 97, 9, pp. 4627-4631.

Lee, S.-Y., & Choi, H.-J. (2018). Persimmon leaf bio-waste for adsorptive removal of heavy metals from aqueous solution. *Journal of environmental management*, 209, pp. 382-392.

Li, H.-Y., Sun, S.-N., Zhou, X., Peng, F., & Sun, R.-C., (2015). Structural characterization of hemicelluloses and topochemical changes in Eucalyptus cell wall during alkali ethanol treatment. *Carbohydr. Polym.* 123, pp. 17–26

Low, M.J.D. (1960). Kinetics of Chemisorption of Gases on Solids, *Chem. Rev.* 60, pp.267-312,

Ma, J., Yang, M., Yu, F., & Zheng, J., (2015). Water-enhanced removal of ciprofloxacin from water by porous graphene hydrogel. *Sci. Rep.* 5, 1, https://doi.org/10.1038 /srep 13578

Mckay, G., Blair, H., & Gardner, J. (1983). The adsorption of dyes in chitin. III. Intraparticle diffusion processes. Journal of Applied Polymer Science, 28, 5, pp. 1767-1778.

Merzouk, B., Yakoubi, M., Zongo, I., Leclerc, J.-P., Paternotte, G., Pontvianne, S., & Lapicque, F. (2011). Effect of modification of textile wastewater composition on electrocoagulation efficiency. *Desalination,* 275, 1, 3, pp.181-186.

Mizuta, K., Matsumoto, T., Hatate, Y., Nishihara, K., & Nakanishi, T. (2004). Removal of nitrate-nitrogen from drinking water using bamboo powder charcoal. *Bioresource technology*, 95, 3, pp. 255-257.

Mohamed, N. R., Ali, M. H., El-Sayed, E. O., & Adel, A . M. (2024). Marble/granite composite to remove lead and cadmium from contaminated water. *Aswan University Journal of Environmental Studies,* 5, 2, pp. 177-201

Odiongenyi, A. O. (2019). Removal of ethyl violet dye from aqueous solution by graphite dust and nano graphene oxide synthesized from graphite dust. *Communication in Physical Sciences*, 4, 2, pp. 103–109.

Odiongenyi, A. O., & Afangide, U. N. (2019). Adsorption and thermodynamic studies on the removal of congo red dye from aqueous solution by alumina and nano-alumina. *Communication in Physical Sciences,* 4, 1, pp. 1–7.

Ogoko, E. C., Kelle, H. I., Akintola, O., & Eddy, N. O. (2023). Experimental and theoretical investigation of *Crassostrea gigas* shells based CaO nanoparticles as a photocatalyst for the degradation of bromocresol green dye (BCGD) in an aqueous solution. *Biomass Conversion and Biorefinery.* https://doi.org /10.1007 /s13399-023-03742-8

Pal, M., Ayele, Y., Hadush, M., Panigrahi, S., & Jadhav, V. J. (2018). Public health hazards due to unsafe drinking water. *Air Water Borne Dis*, 7(1000138), 2.doi:10.4172/2167-7719.1000138

Renugadevi, N.,Sangeetha, R.,& Lalitha, P.(2011). Kineticsof the adsorption of methylene blue from an industrial dyeing effluent onto activated carbon prepared from the fruits of mimusop Elengi. *Archives of Applied Science Research*, 3, 3, , pp. 492-498.

Senberber, F., Yildirim, M., Mermer, N., & Derun, E. (2017). Adsorption of Cr (III) from aqueous solution using borax sludge. *Acta Chimica Slovenica,* 64(3).

Soliman, N. K. & A. Moustafa (2020). "Industrial solid waste for heavy metals adsorption features and challenges; a review." *Journal of Materials Research and Technology,* 9(5): pp. 10235-10253.

Wazwaz, A., Al-Salaymeh, A., & Khan, M. S. (2019). Removing heavy metals through different types of soils and marble powder found in Oman. *Journal of Ecological Engineering,* 20, 4, pp. 136-142.

Weber Jr, W. J., & Morris, J. C. (1963). Kinetics of adsorption on carbon from solution. *Journal of the sanitary engineering division,* 89(2), pp. 31-59.

World Health Organization. (2000). Fifty-third report of the joint FAO/WHO expert committee on food additives. *WHO Technical Report Series,* 896, pp. 1-136.

Yeganeh, G., Ramavandi, B., Esmaeili, H., & Tamjidi, S. (2019). Dataset of the aqueous solution and petrochemical wastewater treatment containing ammonia using low cost and efficient bio-adsorbents. *Data in brief*, 26, 104308. https://doi.org/10.1016/j.dib.2019.104308

Zacaroni, L. M., Magriotis, Z. M., das Graças Cardoso, M., Santiago, W. D., Mendonça, J. G., Vieira, S. S., & Nelson, D. L. (2015). Natural clay and commercial activated charcoal: Properties and application for the removal of copper from cachaça. *Food control,* 47, pp. 536-544.

Zhang, J., & Stan forth, R. (2005). Slow Adsorption Reaction between Arsenic Species and Geothite. Diffusion or Heterogeneous Surface Reaction Control, *Langmuir* 21, pp. 2895- 2901.

Zhu, J., Baig, S. A., Sheng, T., Lou, Z., Wang, Z., & Xu, X. (2015).Fe3O4 and MnO2 assembled on honeycomb briquette cinders (HBC) for arsenic removal from aqueous solutions, *J. Hazard. Mater.* 286, pp. 220–228

Declaration

Consent for publication

Not Applicable

Availability of data and materials

The publisher has the right to make the data public

Conflict of Interest

The authors declared no conflict of interest

Ethical Considerations

Not applicable

Competing interest

The authors report no conflict or competing interest

Funding

The author declared no source of funding

Author Contributions

J. C. Ariwa conceived and supervised the study and contributed to the experimental design. O. K. Amadi carried out the laboratory experiments, data collection, and initial analysis. I. A. Okoro assisted with material preparation, adsorption experiments, and characterization analysis. N. I. Onaka contributed to data interpretation, literature review, and manuscript preparation and revision. All authors read and approved the final manuscript.